The Compact Muon Solenoid Experiment
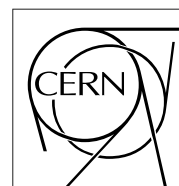
CMS Note

Mailing address: CMS CERN, CH-1211 GENEVA 23, Switzerland

Characteristics and SPICE simulation of a single-sided, n^+ on n Si strip detector before and after neutron irradiation

M. M. Angarano, A. Bader, D. Creanza, M. de Palma, D. Diacono, S. My, G. Raso, P. Tempesta

INFN and University of Bari, Bari, Italy

Abstract

Capacitance, resistance and current measurements were carried out on single-sided, n^+ on n silicon strip detectors. We studied the type inversion after irradiating the detectors with neutron fluences up to $8.3 \cdot 10^{13} \; neutron/cm^2$. To understand the macroscopic irradiation effects, a SPICE model of the detector was developed. By modelling the set-up of the capacitance measurements, our model was able to reproduce the measured frequency dependence of the relevant capacitances both for non-irradiated and irradiated detectors.

1 Introduction

Capacitance values of silicon microstrip detectors are very important parameters which effects their performance. In AC-coupled devices the charge induced on an implanted strip is shared among the coupling capacitance to the read-out electronics and other parasitic capacitances such as the interstrip and body capacitance [1,2]. Therefore, to avoid significant signal loss the coupling capacitance should be as high as possible with respect to other capacitances. The overall noise of the system depends also on the capacitance parameters of the detector [2,3]. The major component is the noise of the readout electronics which is determined by the total detector capacitance seen by the preamplifier. Beside the capacitance values, signal processing and other noise components depend on the resistance values of the detector elements, as well. Impedance due to inductance is negligibly small in Si microstrip detectors, so, in this paper, we will leave it out of consideration.

In many cases, measurements of the specific parameters of Si microstrip detectors is not easy. One of the main difficulties is that resistance and capacitance cannot be measured separately. A further problem is that the capacitance values are usually very small. The typical coupling capacitance is about 100 pF, while interstrip and body capacitances are only a few pF, so these measurements require very sensitive instruments. Moreover, the detector elements behave as a transmission line resulting in a measured capacitance value which depends on the frequency. A possible way to extract the real capacitance and resistance values is to simulate the detector with a proper R-C network (detector model) which is able to reproduce the frequency dependence of the measured capacitance.

In high-energy experiments Si microstrip detectors are mostly used in the central tracking systems, close to the collision region. Here they can be exposed to high level of radiations, which modify considerably the detector performance. The main radiation damage is caused by neutrons, whose fluence, for example in the experiments proposed for LHC (Large Hadron Collider), is expected to exceed 10^{14} $neutron/cm^2$ [4]. One of the effects is the increase of the leakage current, which affects the noise. The doping concentration is also changing during irradiation and even type inversion of the substrate can be reached [5]. Though the radiation damage mechanism can be understood adequately only at microscopic level, these effects induce also variations of macroscopic parameters such as capacitance and resistance values. The aim of our work was to study the change of capacitance and resistance parameters in n^+ on n Si strip detectors due to neutron irradiation.

To have a better understanding of the frequency dependent capacitance measurements, we developed a SPICE model of our detector. This model consists of a simple array of capacitors and resistors. Though all radiation effects cannot be described only by changing resistance and capacitance values, such a model helps to understand what happens in an irradiated device. SPICE simulation is also very effective to determine those capacitance and resistance parameters of the detector that can not be measured directly or whose measured values depend on the surrounding network.

2 Detector description

The subject of the present study is a single-sided, AC coupled detector with n^+ strips implanted over an n type substrate and a plain p^+ layer at the back. It has been produced by SINTEF as a prototype for ATLAS [6] and we have studied it as a back-up solution for CMS [4]. The main feature of this detector is that, after type inversion, it can work in partial depletion mode. After type inversion, the depletion region extends from the strips side and at voltages lower than the full depletion voltage (V_{fd}) we still have an active detective zone at the stri-side. This feature may be crutial if the full depletion voltage exceeds the breakdown voltage.

The active area of the detector is 57.4 mm × 57.4 mm, the thickness is 280 μm. The total number of strips is 1025 with a pitch of 56 μm. Every second strips are read out. Isolation between n^+ strips is achieved by using the p-stop technique. The n^+ strips are biased through 2 $M\Omega$ polysilicon resistors, while the p^+ blocking strips are floating during the operation. Coupling capacitors are obtained by a 200 nm SiO_2 plus 100 nm Si_3N_4 layers grown between the implantation strips and the metallization. The main detector parameters are summarized in table 1 and the details can be found in [6].

A set of 5 detectors were irradiated at different fluences with neutrons of the nuclear reactor "Tapiro" in ENEA-Casaccia Laboratory (near Rome), Italy. The energy distribution of the neutron flux is summarized in table 2 [7]. As it can be seen there is a large amount of neutrons at energies below 1 MeV. We normalized the irradiation fluences to 1 MeV equivalent fluences according to:

$$\phi(1MeV) = \frac{\int \phi(E) K_D(E) dE}{K_D(1MeV)},$$

where $K_D(E)$ is the total displacement kerma cross section taken from [8] and $K_D(1MeV) = 9.5 * 10^4 \, eV \, barn$ [9]. In our calculation we assumed that in each energy group of table 2 the neutron distribution is uniform. From these data the hardness parameter

$$k = \frac{\int \phi(E) K_D(E) dE}{K_D(1MeV) \int \phi(E) dE}$$

is found to be $k = 0.24$. In the following we will always refer to 1 MeV equivalent fluences.

Active Area	$57.4 \, mm \times 57.4 \, mm$
Thickness	$280 \, \mu m$
Resistivity	$4 - 8 \, K\Omega \cdot cm$
Number of n^+ strips	1025
Number of read-out strips	512
Pitch	$56 \, \mu m$
Width of n^+ strips	$12 \, \mu m$
Width of p^+ strips	$18 \, \mu m$
Width of Al	$8 \, \mu m$

Table 1: The main parameters of SINTEF detector [6].

Two detectors were irradiated at a fluence of $0.8 * 10^{13} \, n/cm^2$ and then again at a total fluence of $8.3 * 10^{13} \, n/cm^2$; other two detectors were irradiated directly at a fluence of $8.3 * 10^{13} \, n/cm^2$; and one detector at a fluence of $3.7 * 10^{13} \, n/cm^2$. The measured characteristics of the two detectors irradiated at $8.3 * 10^{13} \, n/cm^2$ in two steps were very similar to the measured characteristics of the detectors which were irradiated in one step. Every irradiation was performed at room temperature and without biasing the detectors. After irradiation the detectors were kept at $0° \, C$ except for the time requested for the measurements, which were done at room temperature ($22 - 23° \, C$). In this paper we will refer to these fluences:

$$\phi_0 = 0 \, n/cm^2,$$
$$\phi_1 = 0.8 * 10^{13} \, n/cm^2,$$
$$\phi_2 = 3.7 * 10^{13} \, n/cm^2,$$
$$\phi_3 = 8.3 * 10^{13} \, n/cm^2.$$

3 Measurements

3.1 Leakage current

Current measurements were carried out with an HP 4145B semiconductor parameter analyzer. It has four SMU (Source Monitor Unit), two voltage sources and two voltage monitors. Each SMU can work as voltage source and current monitor or vice-versa. For total and strip leakage current measurements we put three SMU at 0 V on the bias line, on the guard ring and on the strip, and one SMU on the back contact at a variable negative voltage (typically from 0 to -100 V). After irradiation we expect an increase of the leakage current expressed by the formula:

$$\frac{\Delta I_{tot}}{\mathcal{V}} = \alpha \Phi,$$

where I_{tot} is the leakage current, $\mathcal{V}$ is the active volume of the detector and α is an empirical damage costant whose value is, immediately after irradiation, $\alpha_0 = 5 \div 10 * 10^{-17} A/cm$ and decreases to approximately $\alpha_\infty = 3 * 10^{-17} A/cm$ after all annealing has ceased. At room temperature, α_∞ is achieved approximately 20 days after the end of irradiation [10,11]. The leakage current, in our case, was measured within a few days after irradiation and the detectors were kept cold for all the time after irradiation avoiding any annealing. Therefore, fitting values of our whole set of detectors we obtained $\alpha_0 = 7.1 * 10^{-17} A/cm$.

The first test after irradiation aimed to verifying if the detector substrate reached or not type inversion. Before type inversion, n^+ strips are effectively isolated at a voltage (in absolute value) just greater than V_{fd}. At lower voltages, they are connected via the non-depleted n substrate, so the current measured on a strip at a voltage lower than V_{fd} comes from an effectively large area of the detector. One measures the "true" leakage current of a single strip only

Group	$E_{min}(eV)$	$E_{max}(eV)$	$n/s * cm^2$
1	$3.68 * 10^6$	$1.45 * 10^7$	$7.32 * 10^6$
2	$2.23 * 10^6$	$3.68 * 10^6$	$2.12 * 10^7$
3	$1.35 * 10^6$	$2.23 * 10^6$	$7.38 * 10^7$
4	$8.21 * 10^5$	$1.35 * 10^6$	$3.67 * 10^8$
5	$4.98 * 10^5$	$8.21 * 10^5$	$1.40 * 10^9$
6	$3.02 * 10^5$	$4.98 * 10^5$	$2.78 * 10^9$
7	$1.83 * 10^5$	$3.02 * 10^5$	$3.36 * 10^9$
8	$1.11 * 10^5$	$1.83 * 10^5$	$3.53 * 10^9$
9	$6.74 * 10^4$	$1.11 * 10^5$	$3.26 * 10^9$
10	$4.09 * 10^4$	$6.74 * 10^4$	$3.21 * 10^9$
11	$2.48 * 10^4$	$4.09 * 10^4$	$2.05 * 10^9$
12	$1.50 * 10^4$	$2.48 * 10^4$	$1.97 * 10^9$
13	$9.12 * 10^3$	$1.50 * 10^4$	$1.80 * 10^9$
14	$5.53 * 10^3$	$9.12 * 10^3$	$2.12 * 10^9$
15	$3.36 * 10^3$	$5.53 * 10^3$	$1.52 * 10^9$
16	$2.04 * 10^3$	$3.36 * 10^3$	$7.71 * 10^8$
17	$1.23 * 10^3$	$2.04 * 10^3$	$1.20 * 10^9$
18	$7.48 * 10^2$	$1.23 * 10^3$	$8.43 * 10^8$
19	$4.54 * 10^2$	$7.48 * 10^2$	$4.51 * 10^8$
20	$2.75 * 10^2$	$4.54 * 10^2$	$2.96 * 10^8$
21	$1.01 * 10^2$	$2.75 * 10^2$	$4.21 * 10^8$
22	$2.26 * 10^1$	$1.01 * 10^2$	$5.16 * 10^8$
23	$3.06 * 10^0$	$2.26 * 10^1$	$3.95 * 10^8$
24	$4.14 * 10^-1$	$3.06 * 10^0$	$9.51 * 10^7$
25	0	$4.14 * 10^-1$	$1.90 * 10^6$

Table 2: The energy distribution of the neutron radiation at nuclear reactor "Tapiro", ENEA-Casaccia Laboratory, Italy.
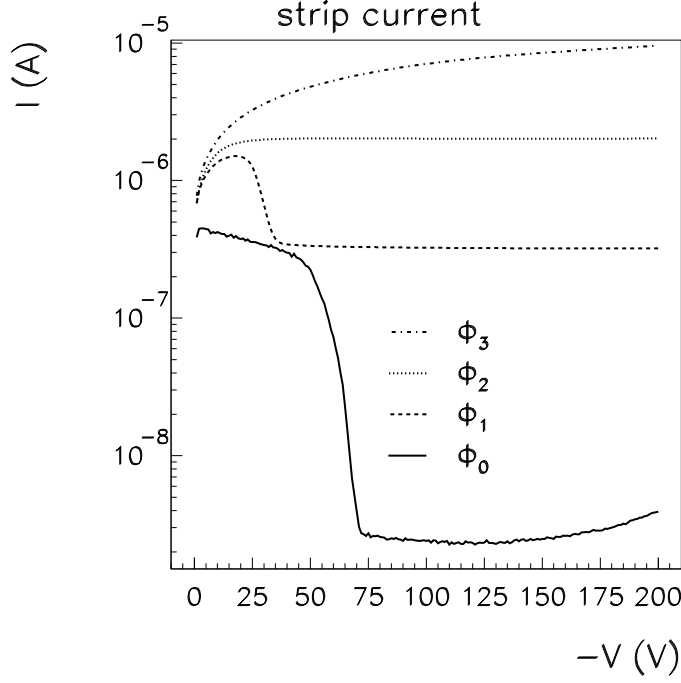
Figure 1: The strip current vs. back voltage at four fluences: $\phi_0 = 0 \ n/cm^2$, $\phi_1 = 0.8 * 10^{13} \ n/cm^2$, $\phi_2 = 3.7 * 10^{13} \ n/cm^2$ and $\phi_3 = 8.3 * 10^{13} \ n/cm^2$.

when the bias voltage exeeds V_{fd}, the full depletion voltage. As a consequence, a sharp decrease at V_{fd} can be observed in the strip current vs. back voltage. After type inversion the detector becomes an $n^+/p/p^+$ detector, the junction side is the strip-side and a small negative voltage on the back is sufficient to deplete the interstrip region and produce isolation between the strips. Therefore, the strip current vs. back voltage curve for an inverted detector does not decrease at V_{fd}. It reaches immediately a plateau value which is the effective strip leakage current. This effect can be seen in figure 1, where one can see that detectors irradiated at fluences ϕ_0 and ϕ_1 are not inverted, while detectors at ϕ_2 and ϕ_3 reached inversion.

3.2 Resistance measurements

For a more complete characterization we also measured some of the resistance parameters of the detector.

The polysilicon resistors connecting the strips to the bias line were not damaged by neutron irradiation and their values remained around $2 \ M\Omega$ at any fluence.

This is not the case for the interstrip resistance, as can be seen in the plot of interstrip resistance vs. back voltage (fig. 2). For non-inverted detectors, similarly to the strip leakage current, the interstrip resistance is low before full depletion and reaches its plateau value at V_{fd}; in inverted detectors, on the other hand, the strips are isolated already for a small back voltage and so interstrip resistance reaches immediately its plateau value. From fig. 3 one can also see that the interstrip resistance (R_{nn}) decreases after irradiation from about $10 \ G\Omega$ to about $20 \ M\Omega$. It is remarkable that this value is the same for all irradiated detectors independently from fluence.

We also measured the resistance values between the strips and the back side, R_{nb}, the implantation - metal strip resistance, R_{nm}, and the proper resistance of the metal strip R_m which is needed for the detector simulation (see the measured values in table 3). The resistance values were obtained as $\Delta V/\Delta I$ at a voltage of $V_{fd} + 25 \ V$.

3.3 Full depletion voltage and breakdown voltage

The full depletion voltage can be extracted from the plot of strip current vs. back voltage (figure 1) as in [12]. In the case of non-inverted detectors V_{fd} is defined as the voltage value at which the strip current reaches its lowest value after the sharp decrease (see fig. 1). In the inverted detectors, V_{fd} is extracted from the C-V measurements.
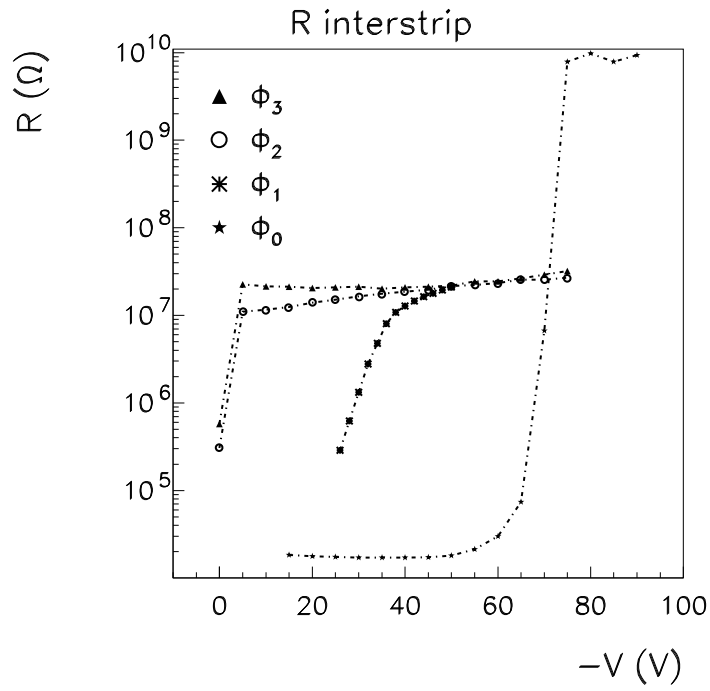
5

Figure 2: The interstrip resistance vs. back voltage at four fluences: $\phi_0 = 0 \ n/cm^2$, $\phi_1 = 0.8 * 10^{13} \ n/cm^2$, $\phi_2 = 3.7 * 10^{13} \ n/cm^2$ and $\phi_3 = 8.3 * 10^{13} \ n/cm^2$.
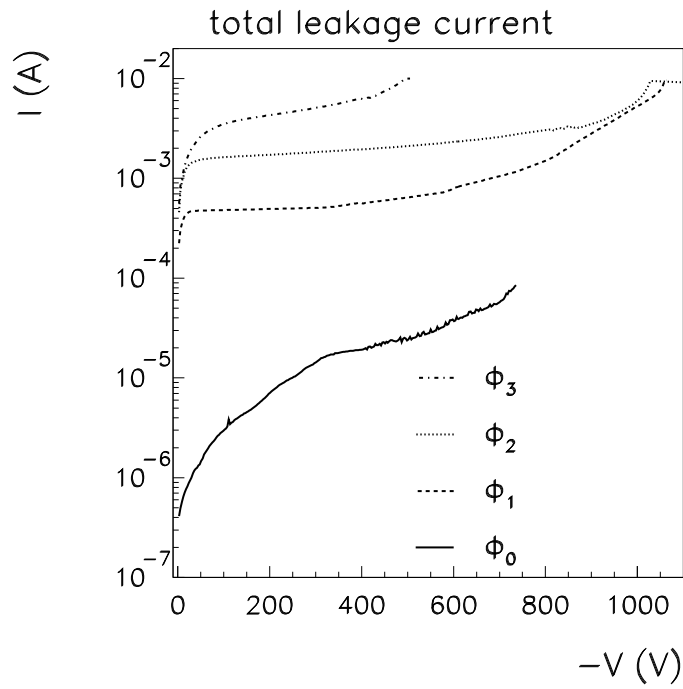

Figure 3: The total leakage current vs. back voltage at four fluences: $\phi_0 = 0 \ n/cm^2$, $\phi_1 = 0.8 * 10^{13} \ n/cm^2$, $\phi_2 = 3.7 * 10^{13} \ n/cm^2$ and $\phi_3 = 8.3 * 10^{13} \ n/cm^2$.

6

Neutron Fluence	$0\,n/cm^2$	$8 \times 10^{12}\,n/cm^2$	$3.7 \times 10^{13}\,n/cm^2$	$8.3 \times 10^{13}\,n/cm^2$
V_{fd}	$75\,V$	$35\,V$	$15\,V$	$100\,V$
V_{break}	$700\,V$	$1050\,V$	$900\,V$	$500\,V$
N_{eff}	$1.26 \times 10^{12}\,cm^{-3}$	$0.59 \times 10^{12}\,cm^{-3}$	$-0.34 \times 10^{12}\,cm^3$	$-2.85 \times 10^{12}\,cm^3$
$I_{tot}(V_{fd} + 25\,V)$	$3.8\,\mu A$	$385\,\mu A$	$1.7\,mA$	$5.1\,mA$
$I_{strip}(V_{fd} + 25\,V)$	$2.3\,nA$	$410\,nA$	$1.9\,\mu A$	$6.2\,\mu A$
$R_{nn}(V_{fd} + 25\,V)$	$12\,G\Omega$	$23\,M\Omega$	$21\,M\Omega$	$19\,M\Omega$
$R_{nm}(V_{fd} + 25\,V)$	$5\,T\Omega$	$--$	$--$	$500\,G\Omega$
$R_{nb}(V_{fd} + 25\,V)$	$70\,G\Omega$	$--$	$--$	$100\,M\Omega$
$R_{polysilicon}$	$2\,M\Omega$	$2\,M\Omega$	$2\,M\Omega$	$2\,M\Omega$
R_m	$300\,\Omega$	$300\,\Omega$	$300\,\Omega$	$300\,\Omega$
C_{AC}	$155\,pF$	$155\,pF$	$155\,pF$	$155\,pF$
C_{nn}	$6.66\,pF$	$--$	$4.3\,pF$	$2.9\,pF$
C_{mm}	$2.9\,pF$	$--$	$2.3\,pF$	$2.15\,pF$

Table 3: The measured voltage, current, resistance and capacitance values of detector for different neutron fluences. The subscripts n, m and b refer to n^+ implantation strips, metal strips and backplane, respectively.

For the highest fluence the test beam data [13] have been also used to determine the true depletion voltage value. The variation of V_{fd} with the strip number is within a few volts. Using the relation:

$$V_{fd} = \frac{|N_{eff}|qd^2}{2\epsilon_{Si}\epsilon_0},$$

one can obtain the value of the effective doping concentration, N_{eff} for all fluences. The measured V_{fd} and the calculated N_{eff} values are summarized in tab. 3. The change of N_{eff} due to irradiation can be described by the equation:

$$N_{eff} = N_{eff,0} - N_C(\phi) - N_Y(\phi, t, T),$$

where $N_{eff,0}$ is the effective doping concentration before irradiation, $N_C(\phi)$ is the stable defect term and $N_Y(\phi, t, T)$ is the annealing term. Our measurements were performed immediately after the irradiation, so we can neglect the annealing term and consider only the stable defect term:

$$N_C(\phi) = N_{C0}(1 - e^{-c\phi}) - g_C\phi,$$

where N_{C0} is related to the initial donor concentration (and so to $N_{eff,0}$) while c and g_C are two parameters related respectively to the donor removal and to the acceptor like defects introduction. In table 4 we compare the measured and calculated V_{fd} values at different fluences. The calculated values were obtained using $c = 2.29 * 10^{-13}\,cm^2$ and $g_C = 2.5 * 10^{-2}\,cm^{-1}$ and $N_{C0} = (0.5 \pm 0.15)N_{eff,0}$, which were measured on comparable wafers [14].

In high radiation environment the breakdown voltage (V_{break}) may become a limiting factor for the detector operation. Fig. 3 shows the total leakage current as a function of the back voltage, from which the breakdown voltage can be determined. Our definition of V_{break} is the voltage at which an increase of $\Delta V = 5\,V$ results in 10 % increase of the leakage current. Fig. 4 shows the values of the breakdown and full depletion voltage versus fluence. The theoretical formula of V_{break}^a (avalanche breakdown) for a one-sided ideal step junction has the form:

$$V_{break}^a = \frac{\epsilon_{Si}\epsilon_0 \mathcal{E}_1^2}{2qN_{eff}},$$

where $\mathcal{E}_1$ is the critical value of the electric field [15]. Obviously, this formula does not hold for such a complex structure as a microstrip detector, but the main feature, that V_{break} is inversely proportional to N_{eff}, is still valid. Fig. 4 shows that the breakdown voltage decreases fluence, while the full depletion voltage exhibits the opposite trend.

3.4 Capacitance measurements

The capacitance measurements were carried out with an HP 4284A LCR meter using an HP 4142B power supply for biasing the detector. Fig. 5 shows the experimental setup for the measurement of the coupling capacitance (C_{AC}), the first neighbour DC interstrip capacitance (C_{nn}), the second neighbour DC interstrip capacitance (C_{nn+1}) and the AC interstrip capacitance (C_{mm}).
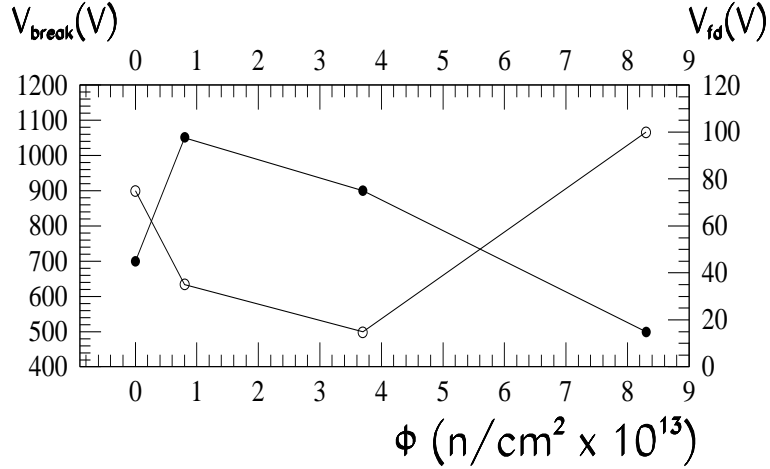
Figure 4: The breakdown voltage (●) and the full depletion voltage (○) vs. fluence.

Fluence	Measured V_{fd} (V)	Calculated V_{fd} (V)
Φ_1	35 ± 1	32 ± 5
Φ_2	15 ± 2	18 ± 11
Φ_3	100 ± 15	86 ± 25

Table 4: The measured and calculated V_{fd}. The uncertainty on the calculated values is due to the 20% uncertainty of the fluence.

Before each kind of measurement we performed the "short" correction on HP 4284A by shorting the cables connected to "high" and "low" terminals as near as possible to the D.U.T. (device under test) and the "open" correction, raising the probe connected to the "low" terminal. The open correction was performed with detector under bias (at the same voltage at which the measurement was performed). We tried all configurations with "short" and/or "open" correction on or off and we found that the effect of "short" correction was negligible and the effect of "open" correction was almost independent from the frequency. Measurements were carried out at various frequencies from 20 Hz up to 1 MHz at a bias voltage $V = V_{fd} + 25\ V$. We shall discuss the frequency dependence of the measured capacitance in section 4. Plateau values of the measured capacitance are summarized in table 3.

The measured C_{AC} values do not change with fluence. On the other hand, C_{nn} and, as a consequence [1], C_{mm} decrease after irradiation (see figure 6a, 6b).

This effect is not completely clear, but it is probably due to the change of the p-stop potential. In our detector it was not possible to measure the p-stop voltage, but other results [16] showed that, due to the change of the resistance values in irradiated detectors, the voltage between the p-stops and the n^+ strips increases after irradiation. As a consequence, also the depletion layer between the n^+ and p^+ implantation strips increases, which results in lower capacitance.

In non-inverted detectors the n^+ strips are connected to the bias line (which are grounded in the capacitance measurements) through the polysilicon resistors, whose value is considerably lower than the resistance towards the back and p-stops, so that they are at a voltage close to 0 V. The p-stop potential is close to the n^+ strip voltage before full depletion, but for higher (in absolute value) back voltages it starts to increase (in absolute value) approximately linearly [16]. If the p-stop voltage increases the depleted region between the n^+ strip and the p-stop also increases and, as a consequence, C_{nn} decreases (fig. 7 a).

In the case of inverted detectors the p-stop voltage starts to increase as soon as the detector is biased, so at full depletion there is a considerable voltage difference between the n^+ strips and the p-stops, yielding C_{nn} lower than in non-inverted detectors. A further increase of the back voltage increases the p-stop voltage and, as a consequence, C_{nn} decreases until the interstrip region is fully depleted (fig. 7 b). Unfortunately the measurement set-up was

---

[1] The measurements of C_{mm} were carried out, in fact, for testing the SPICE simulation. C_{mm} depends both on C_{AC} and C_{nn}, so its change after irradiation is due to the changes of C_{nn}, being C_{AC} unchanged.
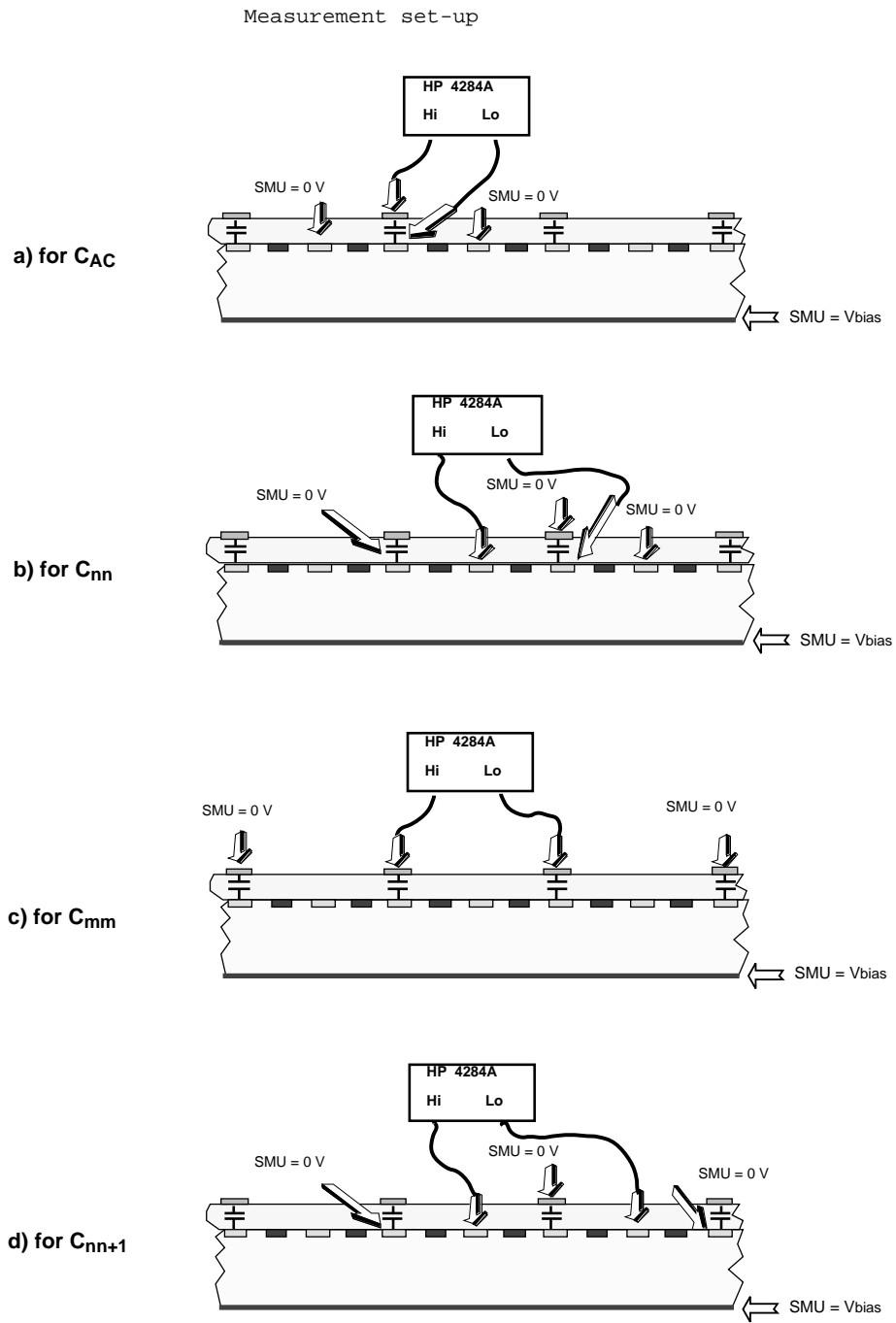
Measurement set-up

HP 4284A

Hi   **Lo**

SMU = 0 V   SMU = 0 V

a) for C_AC

SMU = Vbias

HP 4284A

Hi   **Lo**

SMU = 0 V   SMU = 0 V   SMU = 0 V

b) for C_nn

SMU = Vbias

HP 4284A

Hi   **Lo**

SMU = 0 V   SMU = 0 V

c) for C_mm

SMU = Vbias

HP 4284A

Hi   **Lo**

SMU = 0 V   SMU = 0 V   SMU = 0 V

d) for C_nn+1

SMU = Vbias

Figure 5: The measurement set-up of **a)** the coupling capacitance, **b)** the DC interstrip capacitance, **c)** the AC interstrip capacitance and **d)** the second neighbour DC interstrip capacitance.
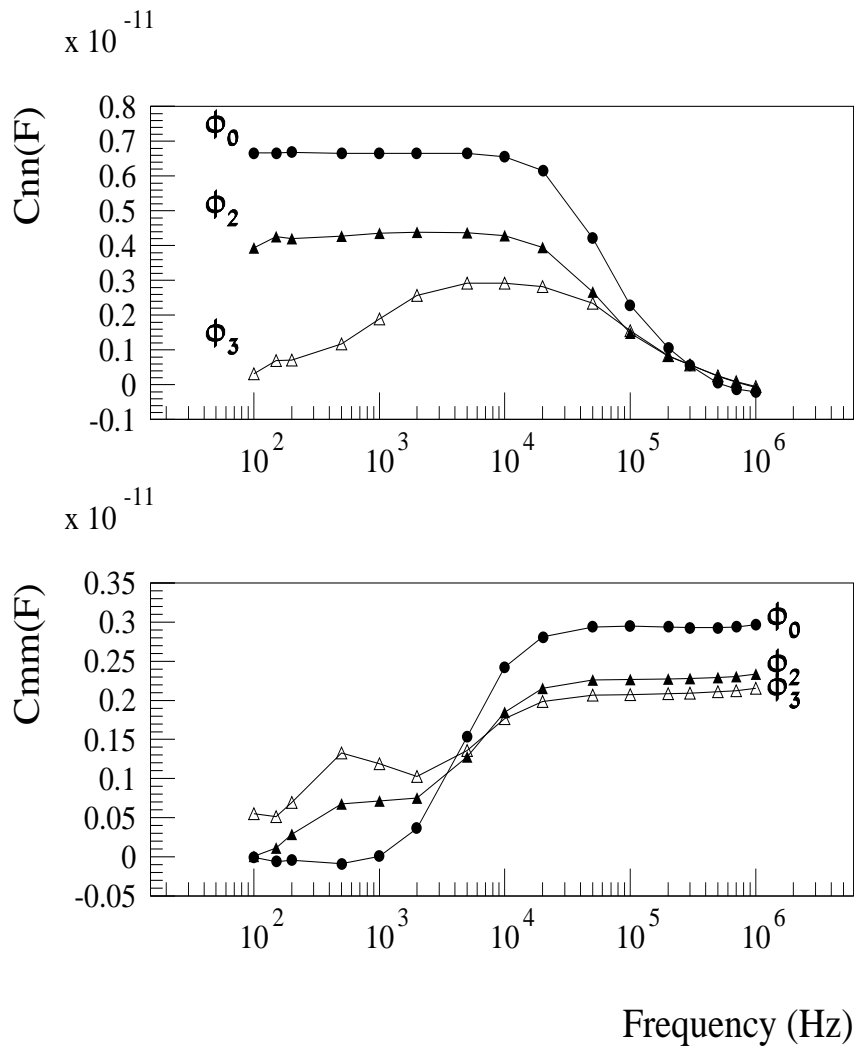
Figure 6: Frequency dependent capacitance measurements performed at three different neutron fluences: $\phi_0 = 0\ n/cm^2$, $\phi_1 = 0.8 * 10^{13}\ n/cm^2$, $\phi_2 = 3.7 * 10^{13}\ n/cm^2$ and $\phi_3 = 8.3 * 10^{13}\ n/cm^2$. **a)** DC interstrip capacitance, **b)** AC interstrip capacitance.
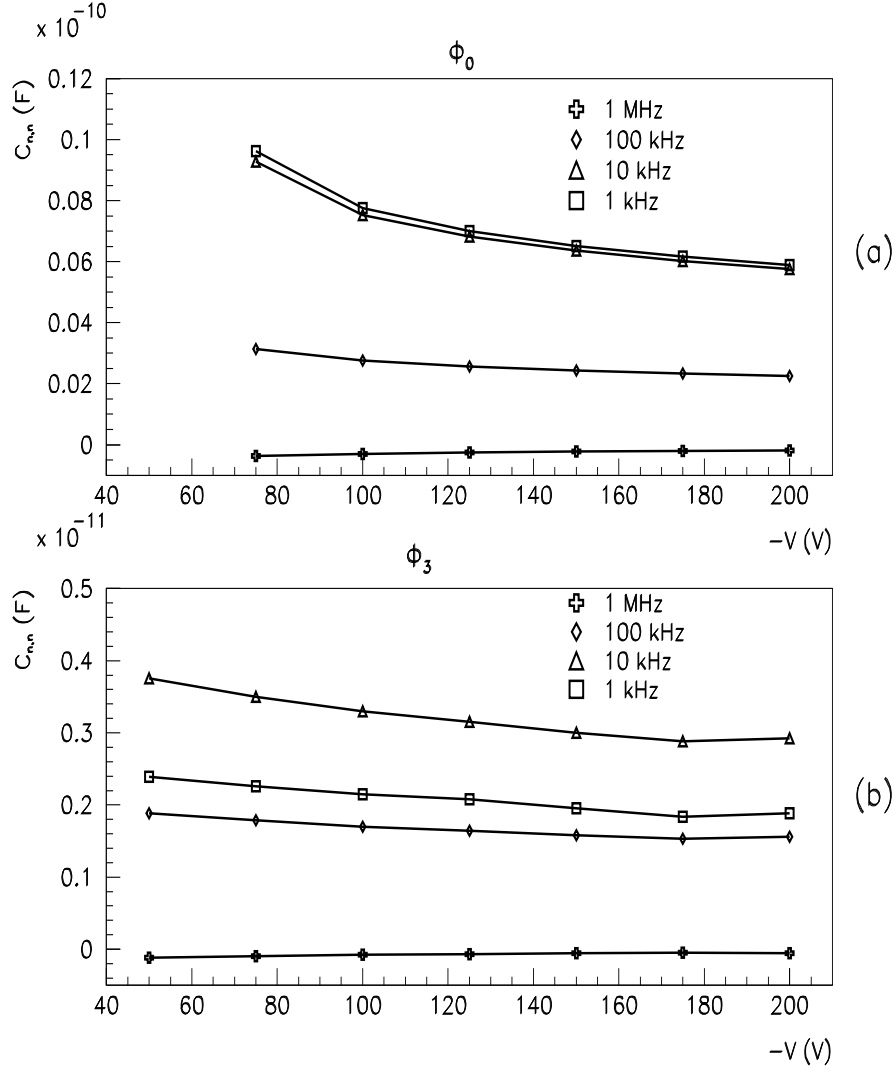
Figure 7: The DC interstrip capacitance vs. back voltage at four frequencies, **a)** before irradiation, **b)** after irradiation at a neutron fluence of $\phi_3 = 8.3 * 10^{13}\ n/cm^2$.

limited to maximum voltage of about $200\ V$, and it seems that C_{nn} still have not reached its minimum value.

We also measured C_{nn+1} but the capacitance value as a function of the frequency did not show any plateau. It was not possible to measure C_{nb} due to its small value and to network effects.

4   SPICE simulation and interpretation of the capacitance measurements

The simplest SPICE model of the detector under test includes 4 read-out strips and 3 floating strips, so 7 n^+ implantation strips were simulated alltogether. For each n^+ strips, the model contains AC coupling ($\mathfrak{C}_{AC}$), body ($\mathfrak{C}_{nb}$) and interstrip ($\mathfrak{C}_{nn}$) capacitors. In addition, each n^+ strip is capacitatively coupled to its second neighbour n^+ strips, whose capacitance is denoted by $\mathfrak{C}_{nn+1}$. We use Gothic letters ($\mathfrak{C}$ for capacitance, $\mathfrak{R}$ for resistance) to distinguish the parameters of the SPICE model from the measured values. The scheme of the detector cross section with the capacitive couplings can be seen in figure 8 a. The resistance between the elements of the detector and the strip resistance itself were also taken into account in our model. The resistances between the metal strip and the n^+ strip is denoted by $\mathfrak{R}_{mn}$, while the other resistance parameters are denoted by $\mathfrak{R}_{nn}$, $\mathfrak{R}_{nn+1}$ etc., similarly to the capacitance values.

The network simulating the detector is built up from 342 unit cells (60 cells/cm) of capacitors and resistors. One
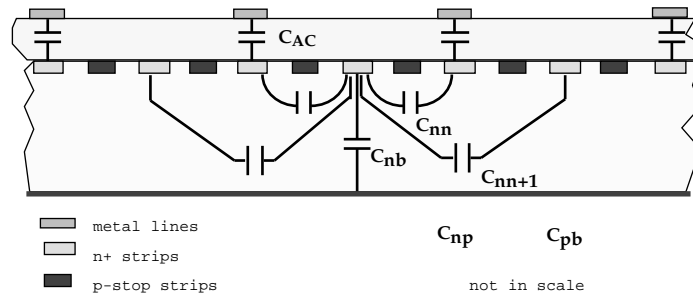
metal lines

n+ strips

p-stop strips

C_{AC}

C_{nn}

C_{nb}

C_{nn+1}

C_{np} C_{pb}

not in scale

Figure   8,a

metal lines

n+ strips

p-stop strips

C_{AC}

C_{np}

C_{nb}
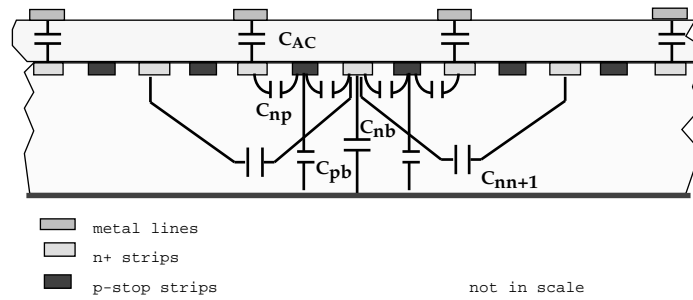
C_{pb}

C_{nn+1}

not in scale

Figure   8,b

Figure 8: The schematic cross section of the detector. The figure shows the capacitive couplings between the detector elements that were included in the SPICE simulation. **a)** "simple" model, without p-stops, **b)** "extended" model, featuring also the p-stop couplings.

cell of the detector can be considered as a slice (perpendicular to the strips) of the detector. The complete model of the detector contains more than 30000 circuit elements. By simulating the measurements of capacitance, we found empirically that 60 cells/cm is the minimum number of cells to reproduce the measured data.

The choice of using 342 unit cells to describe the detector determined by the frequency dependence of capacitance measurements. The capacitances C_{AC}, C_{nn}, C_{nn+1} exhibit a plateau value at low frequency and decrease at higher frequencies (see figure 9 a,b and d) [1]. This effect is due to the resistance of the implantation strips. Let us consider, for example, the measurement of C_{AC}: due to the presence of the implantation strip resistance, the coupling of the metal and implantation strips is equivalent to a lot of high-pass filters connected in parallel (in our model 342 simple filters). At low frequencies the signal applied through the "high" probe of the LCR meter spreads along the total lenght of the strip, so the total capacitance can be measured. As the frequency increases the signal starts to be filtered after the first stages and only part of the total strip capacitance is measured: as a consequence, a drop of the measured capacitance value is observed. The behaviour of C_{nn} and C_{nn+1} at high frequencies is similarly determined by the resistance of the implantation strip (the resistance of the metal strip being negligibly small).

In the SPICE model, whenever available, we used the measured values for the resistance of the implant (table 3). Those resistance values that can not be measured and all capacitance values were free parameters and were determined in the fitting procedure.

First we simulated the capacitance measurements performed on a *non-irradiated* detector. With our SPICE model, we simulated C_{AC}, C_{nn}, C_{mm} and C_{nn+1} capacitance measurements (see figure 5). In this case it was possible to reproduce the experimental curves (dashed line in figure 9). These curves were obtained using the same set of parameter values, which are listed in the first column of table 5. The resistance of the implantation strip, R_n can not be measured on our detector, and C_{nb} and C_{nn+1} measurements do not have plateau values, so we were able to determine these parameters only by SPICE simulation.

	Before irradiation		After irradiation	
	without p^+ stops	with p^+ stops	without p^+ stops	with p^+ stops
$\Re_{polysilicon}$	$2\,M\Omega$	$2\,M\Omega$	$2\,M\Omega$	$2\,M\Omega$
$\Re_n$	$37\,K\Omega$	$37\,K\Omega$	$37\,K\Omega$	$37\,K\Omega$
$\Re_m$	$300\,\Omega$	$300\,\Omega$	$300\,\Omega$	$300\,\Omega$
$\Re_{nm}$	$5\,T\Omega$	$5\,T\Omega$	$500\,G\Omega$	$500\,G\Omega$
$\Re_{nn}$	$12\,G\Omega$	$13.8\,G\Omega$	$20\,M\Omega$	$23\,M\Omega$
$\Re_{nb}$	$70\,G\Omega$	$70\,G\Omega$	$100\,M\Omega$	$100\,M\Omega$
$\Re_p$	∞	$592\,K\Omega$	∞	$592\,K\Omega$
$\Re_{np}$	∞	$48\,G\Omega$	∞	$80\,M\Omega$
$\Re_{pb}$	∞	$70\,G\Omega$	∞	$10\,M\Omega$
$\mathfrak{C}_{AC}$	$155\,pF$	$155\,pF$	$155\,pF$	$155\,pF$
$\mathfrak{C}_{nn}$	$6.66\,pF$	$1\,pF$	$3.6\,pF$	$1\,pF$
$\mathfrak{C}_{nn+1}$	$0.55\,pF$	$0.55\,pF$	$0.63\,pF$	$0.65\,pF$
$\mathfrak{C}_{mm}$	0	0	$0.2\,pF$	$0.5\,pF$
$\mathfrak{C}_{nb}$	$2.23\,pF$	$1.2\,pF$	$2.23\,pF$	$1.2\,pF$
$\mathfrak{C}_{np}$	0	$11.9\,pF$	0	$5.2\,pF$
$\mathfrak{C}_{pb}$	0	$1.8\,pF$	0	$1.8\,pF$

Table 5: The resistance and capacitance parameters of the SPICE model which resulted as the best fit of the capacitance measurements performed on the detector before and after irradiation with a fluence of $\phi_3 = 8.3 * 10^{13}\,n/cm^2$ (see figure 9 and 10).

We also fitted the capacitance measurements performed on the detector *irradiated* at the highest fluence ($\phi_3 = 8.3 * 10^{13}\,n/cm^2$). This detector has reached type inversion and the frequency dependence of the capacitance values changed considerably (compare figure 9 and 10). The data shown in figure 10 are more difficult to understand only with SPICE simulation because they can also be due to microscopic substrate effects that can not be taken into account by simply changing capacitance and resistance parameters in the model. Our "simple" SPICE model was not able to reproduce the main structures of the capacitance measurements (dashed curves in figure 10).

In an "extended" version of the model we also included the p^+ blocking strips (fig. 8 b). The capacitance between p^+ and n^+ strips and the capacitance between p^+ stops and backplane are denoted by $\mathfrak{C}_{np}$ and $\mathfrak{C}_{pb}$, respectively. In the simple model, $\mathfrak{C}_{nb}$ was found to be approx. a factor of 2 larger than the capacitance value that can be calculated
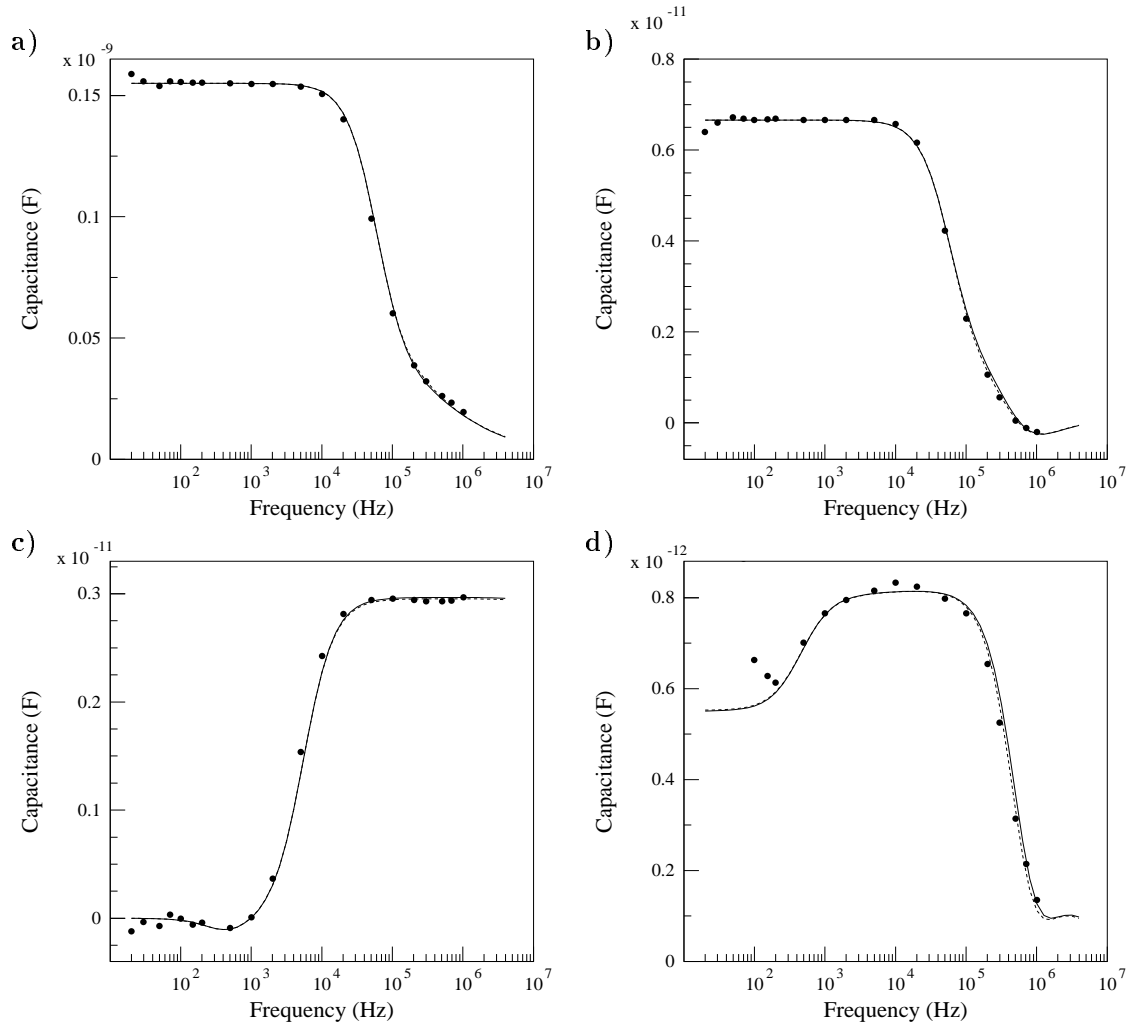
Figure 9: Frequency dependent capacitance measurements performed on the detector *before irradiation*. **a)** AC coupling capacitance, **b)** first neighbour DC interstrip capacitance, **c)** AC interstrip capacitance and **d)** second neighbour DC interstrip capacitance. The solid and dashed lines are the results of the SPICE simulation of the measurements with and without including the p^+ stops in the model, respectively. The fits were obtained with the capacitance and resistance parameters listed in table 5.
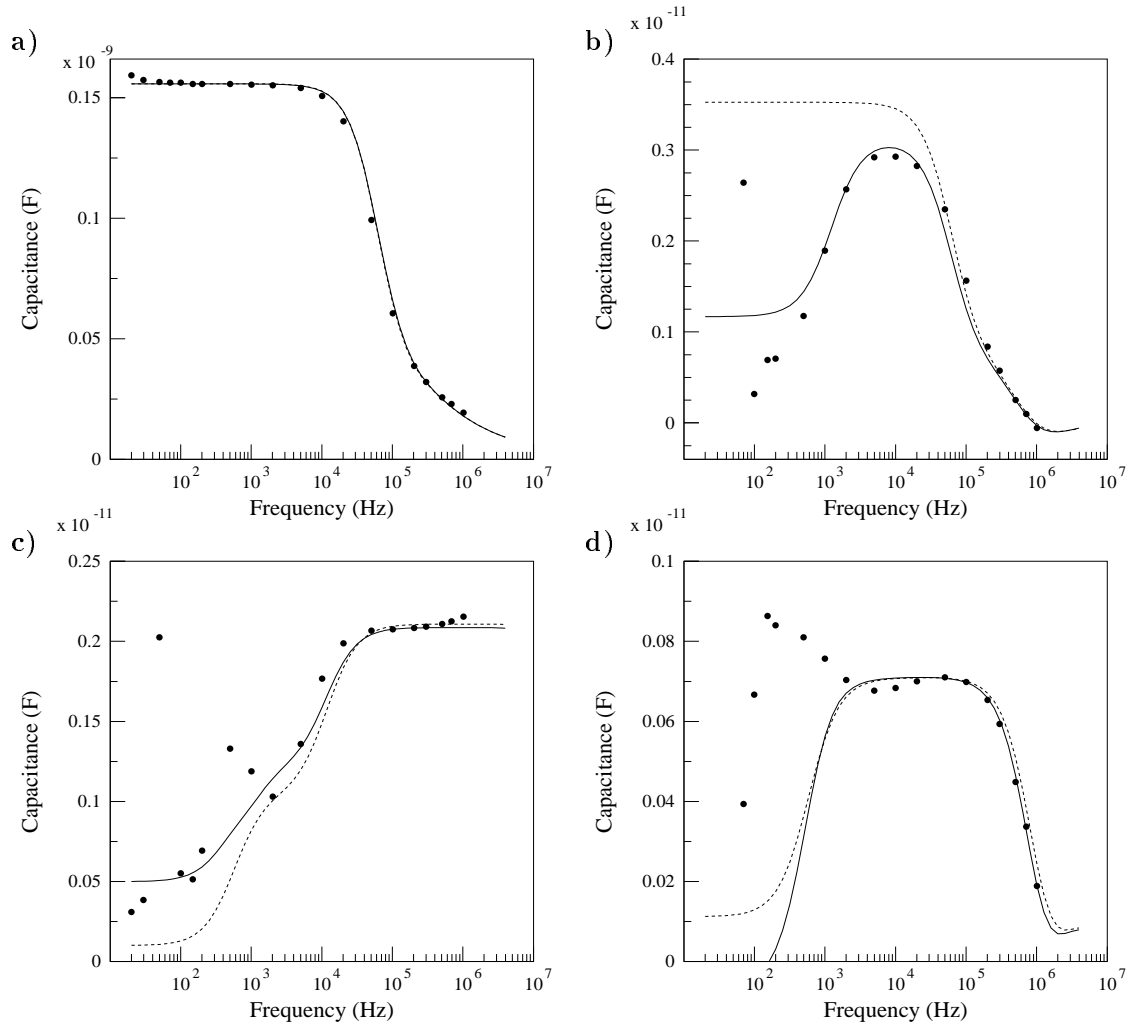
Figure 10: Frequency dependent capacitance measurements performed on the detector *after irradiation* with a neutron fluence of $\phi_3 = 8.3 * 10^{13}\ n/cm^2$. **a)** AC coupling capacitance, **b)** first neighbour DC interstrip capacitance, **c)** AC interstrip capacitance and **d)** second neighbour DC interstrip capacitance. The solid and dashed lines are the results of the SPICE simulation of the measurements with and without including the p^+ stops in the model, respectively. The fits were obtained with the capacitance and resistance parameters listed in table 5.

15

from the geometry of the detector ($C_{nb}^{geom} = 1.2$ pF). After including the p^+ strips we obtained a more realistic value for this parameter (see in table 5). This was the first indication that p^+ stops should be included in the model. With the "extended" model we obtained a better agreement with the C_{nn} measurement in the case of *irradiated* detector (solid lines in figure 10 b and c), while for *unirradiated* detector the difference between the two models was very small (see figure 9).

Unfortunately, even with the extended model, we were not able to understand part of the behaviour of the capacitance measurements particularly in the small frequency region (figure 10 b, c, d).

To summarise our experience of simulating the capacitance measurements with the "extended" model we conclude the following:

1. One of the most important parameter, the coupling capacitance (C_{AC}) depends practically only on $\mathfrak{C}_{AC}$ parameter. The behaviour of the curve at high frequencies, as it was discussed before, is determined by $\mathfrak{R}_n$.

2. The interstrip capacitance is mostly determined by the $\mathfrak{C}_{np}$ parameter: by changing $\mathfrak{C}_{np}$ of 2 pF, the maximum value of C_{nn} in the frequency range between 20 Hz and 1 MHz, changed by about the half. This is because the model contains $\mathfrak{C}_{np}$ capacitors connected in series between the implantation strips. C_{nn} depends also on other capacitance parameters: by decreasing $\mathfrak{C}_{nb}$ and $\mathfrak{C}_{pb}$ by 1 pF, the maximum value of the interstrip capacitance increases of approximately 0.2-0.3 pF. Increasing $\mathfrak{C}_{nn+1}$ of 0.2 pF determines an increase of C_{nn} by about 0.08-0.12 pF.

The decreasing of C_{nn} at frequencies lower than 5 MHz in the case of the *non-irradiated* detector can be attributed to the low interstrip and strip to back resistance. Comparing the value of $\mathfrak{C}_{np}$ parameter before and after irradiation, one can observe the change of this parameter from 13.9 pF to 7.2 pF.

3. The capacitance between two neighbouring metallizations, C_{mm} becomes very small at low frequencies because in this measurement configuration the test signal is shunted to ground through the low ($2\ M\Omega$) polysilicon resistor. At high frequencies, however, the impedance of the capacitance decreases and become measurable (figure 9 c, 10 c). The breakdown of the capacitance curve, therefore, depends mainly on the polysilicon resistance value.

The simulation of C_{mm} is very useful to test the SPICE model because it depends on several capacitance parameters and has a well defined plateau value at the high frequency limit.

In the simulation of *unirradiated* detectors, we did not need any additional capacitors between the metal strips. The measured capacitance is only due to $\mathfrak{C}_{AC}$, $\mathfrak{C}_{nn}$, $\mathfrak{C}_{nb}$ and $\mathfrak{C}_{nn+1}$. In the case of *irradiated* detectors (see figure 10 c), however, it was possible to fit the C_{mm} measurement only by adding a capacitance of $\mathfrak{C}_{mm} = 0.5$ pF directly between the metallization strips. We attribute this effect to the oxide charge of the $SiO_2 - Si$ interface, which effect may also contribute to the low interstrip resistance measured after irradiation.

C_{mm} decreased of approx. 0.3-0.5 pF by increasing $\mathfrak{C}_{nb}$ and $\mathfrak{C}_{pb}$ of 1 pF, and increased of approx. 0.08-0.12 pF by increasing $\mathfrak{C}_{nn+1}$ of 0.2 pF.

4. C_{nn+1} is mainly correlated with $\mathfrak{C}_{nn+1}$ parameter. It was found to be almost independent of the other capacitance parameters: it increased of less than 0.1 pF by changing, for instance, $\mathfrak{C}_{np}$ of 1 pF.

5 Conclusions

As expected, neutron irradiation of n^+ on n Si microstrip detectors has a big effect not only on the working parameters such as V_{fd}, V_{break}, I_{strip}, I_{tot} but also on the resistance and capacitance parameters. Most of the change in the capacitance measurements after irradiation can be attributed to the decrease of the resistance between the strips and between the strips and the backplane.

The irradiation has negligible effect on the coupling capacitance, which is the most important parameter for the signal coupling. On the other hand, interstrip capacitance decreases with increasing the fluence.

It was necessary to include the p^+ blocking strips in our model to describe and understand the main characteristics of the frequency dependent capacitance measurements performed on an irradiated detector after type inversion. In the case of the unirradiated detector a more simple model, which did not contain the p^+ blocking strips, was good enough to describe the capacitance measurements.

We pointed out that the frequency dependence of the measured capacitace is due to the experimental method which does not take into account the complex resistance and capacitance structure of the detector. SPICE simulation can be used to determine unmeasureable capacitance and resistance parameters, as well.

Acknowledgements

References

1. C. LeVier, Capacitance in Silicon Strip Detectors, UC, Santa Cruz, Senior Thesis, SCIIP 92/26.

2. E. Barberis *et al.*, Nucl. Instrum. Meth. A 342 (1994) 90.

3. C. Bozzi, Signal-to-Noise Evaluation for the CMS Silicon Microstrip Detectors, CERN CMS NOTE 1997/026.

4. CMS Technical Proposal, CERN/LHHCC/94-38 (1994).

5. D. Pitzl *et al.*, Nucl. Instrum. Meth. A 311 (1992) 98.

6. The ATLAS Prototype Detector, SINTEF, http://www.oslo.sintef.no/ecy/7230/atlas.html.

7. G. Rosi, Tapiro in ENEA, Casaccia, Italy, private communication.

8. A. M. Ougouag *et al.*, IEEE Trans. Nucl. Sci. vol.37 no.6 (1990) 2219.

9. ASTM E722-85 Standard practice for characterizing neutron fluence spectra in terms of an equivalent monoenergetic neutron fluence for radiation hardness testing of electronics, ASTM E-772-93 (revision 1993).

10. A. Chilingerov *et al.* Nucl. Instr. Meth. A 360 (1995) 432.

11. CMS Collaboration, The Tracker Project, CERN/LHCC 98-6.

12. A. Brandl *et al.*, Nucl. Instr. Meth. A 399 (1997) 76.

13. to be published.

14. H. Feick *et al.*, Nucl. Instr. Meth. A 377 (1996) 217.

15. R. S. Muller T. I. Kamins, Device electronics for integrated circuits, John Wiley and Sons, 1977.

16. RD20 collaboration, Nucl. Instr. Meth. A 362 (1995) 297.